(Received 23 February 2025, Accepted 1 April 2025, Scheduled 7 April 2025)

Eight-Element Dual-Band MIMO Antenna for 5G Smartphone

Yingjian Hou[1], Zhonggen Wang[1,*], Ming Yang[2], and Jinzhi Zhou[3]

[1]*School of Electrical and Information Engineering, Anhui University of Science and Technology, Huainan 232001, China*
[2]*School of Electrical and Communications Engineering, West Anhui University, Luan 237012, China*
[3]*School Electrical and Information Engineering, Bozhou University, Bozhou 236800, China*

ABSTRACT: This study proposes a dual-band MIMO antenna with high element isolation for 5G smartphones. The antenna unit consists of stacked F-shaped radiators, perpendicular to the motherboard, printed on the outer side frames. The antenna feeder is shaped like the Chinese character "工" and is printed on the inner surface of the side substrate. Based on this design, eight F-shaped antenna units are placed at the ends of two long side panels, forming an 8-element MIMO antenna system. High isolation in the operating bands is achieved using ground stubs and defective ground structures (DGSs). All radiating elements are etched on a low-cost FR4 substrate with a total size of $150 \times 75 \times 6.8\,\text{mm}^3$. The antenna system is modeled and measured to operate in the N78 (3.3–3.8 GHz), N79 (4.4–5.0 GHz), and WLAN 5 GHz bands (5.15–5.85 GHz). The isolation between neighboring antenna units is greater than 15 dB, with total efficiencies ranging from 62% to 79%, and a measured envelope correlation coefficient (ECC) of less than 0.01. Additionally, the antenna performance in one-handed and two-handed holding scenarios has been evaluated, showing favorable results. These findings demonstrate that the proposed antenna system is well suited for MIMO applications in 5G smartphones.

1. INTRODUCTION

With the continuous advancement of 5G communication technology [1], the improvement of communication performance of smartphones, as the most common 5G terminal devices, has become the key to the development of the industry. 5G networks offer higher transmission speeds, lower latency, and wider connection density than 4G. The realization of these advantages not only relies on the construction of base stations and network architecture, but is also closely related to the hardware performance of terminal equipment, especially in the design and application of wireless communication antennas.

In 5G smartphones, antenna system plays a crucial role. Traditional single-band antennas can no longer meet the needs of high-speed, high-traffic communications, so the use of multi-frequency bands and multi-antenna systems design has become an effective way to improve the communication capacity of cell phones. Multiple input multiple output (MIMO) antenna technology was born in this context. MIMO technology [2–5] is through the simultaneous use of multiple transmitter and receiver antennas. Multi-antenna system designs [3] and [4] form a 4-unit antenna system by adding antenna units, while both [2] and [5] form an 8-unit antenna system by adding antenna units, while the latter covers the frequency band with better impedance matching. Therefore, in this paper we also consider the use of an 8-unit antenna system.

However, placing multiple antennas in a limited design space may lead to serious degradation of isolation and radiation efficiency of the antenna system. Therefore, how to achieve effective isolation of each antenna in a MIMO system is a major challenge for antenna designers. Several techniques [6–9] have shown that the isolation between antenna elements can be improved when they are closely spaced. The commonly used decoupling methods mainly include: loading floor branches or parasitic units, defective ground structure (DGS) [10–14], neutralization lines [15–18], and other self-decoupling methods.

In this paper, a 5G dual-band MIMO antenna with an operating frequency covering 2.62–3.94 GHz and 4.35–5.98 GHz is proposed with a size of $150 \times 75 \times 6.8\,\text{mm}^3$, which is similar to the appearance of mainstream smartphones such as Huawei Mate 60. The eight elements of the antenna are distributed on two side metal frames, and the coupling effect between the elements is reduced by a decoupling structure (DG). This study designed, fabricated, and tested this MIMO antenna and analyzed its performance metrics, including S-parameters, radiation efficiency, directional map, and envelope correlation coefficient (ECC). The antenna can effectively cover the 5G Chinese bands N78 (3.4–3.8 GHz) and N79 (4.4–5.0 GHz) as well as WLAN 5G (5.15–5.85 GHz), thus reducing the number of antennas dedicated to the WLAN band in 5G handsets. The antenna maintains isolation better than -15 dB across the entire operating band, which meets the performance requirements of 5G terminal antennas. In addition, its overall efficiency is in the range of 62%–79%, which is an excellent performance. The measured data are highly consistent with the simulation results.

2. PROPOSED MIMO ANTENNA SYSTEM

2.1. Antenna Structure

The structure and physical dimensions of the proposed antenna are shown in Fig. 1(a). The MIMO antenna consists of three FR4 substrates with $\varepsilon_r = 4.4$ and $\tan\delta = 0.02$. These substrates include a central main substrate as well as two addi-

* Corresponding author: Zhonggen Wang (zgwang@ahu.edu.cn).

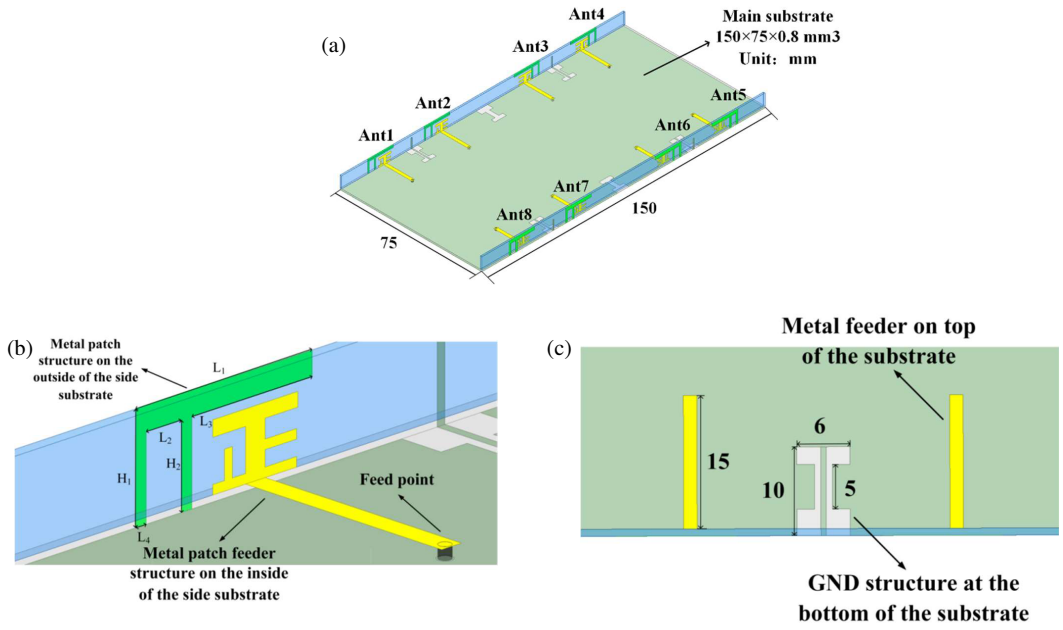

FIGURE 1. Shape and dimensions of the proposed 8-element MIMO antenna. (a) Antenna system. (b) Detailed structure and dimensions of the antenna. (c) Detailed structure of the decoupling structures.

tional side substrates. The dimensions of the main substrate are $150 \times 75 \times 0.8\,\text{mm}^3$, while the dimensions of the side substrates are $150 \times 6 \times 0.8\,\text{mm}^3$. Eight antenna elements, which are designed to be aligned perpendicular to the main substrate, are precisely printed on the two side substrates. The proposed 8-element antenna array (Ant 1-Ant 8) is divided into two 4-element subarrays (Ant 1-Ant 4 and Ant 5-Ant 8) located on the left and right long edges of the metal frame. Among them, Ant 1-Ant 4 and Ant 5-Ant 8 are structurally symmetric. To simplify the discussion, this study mainly focuses on the performance analysis of Ant 1-Ant 4. Table 1 lists the optimum size of the important components of the antenna.

TABLE 1. Optimized parametric dimensions of proposed MIMO antenna.

Parameters	L_1	L_2	L_3	L_4	H_1	H_2
Value (mm)	13.5	2.7	4.2	0.8	6.8	5.3

2.2. Antenna Element

As shown in Fig. 1(b), each antenna unit consists of a heat sink, a feed line, and an "F" shaped patch. The radiator consists of an elongated structure arranged in the shape of a Chinese character "正", comprising three horizontal rectangular microstrip lines and two longitudinal rectangular microstrip lines precisely printed on the inner surface of the side substrates. The "F" patch consists of two horizontal rectangular microstrip lines and one longitudinal rectangular microstrip line loaded on the outer surface of the side substrates. The feed lines are then printed on the upper surface of the main substrate and are connected to the heat sink. Four antenna units are printed on the inner surface of each edge substrate. In order to improve the isolation between the units, a DGS is introduced, which is shown in Fig. 1(c). The decoupling structure consists of a Chinese character "工" shaped slot. These decoupling structures are etched on the bottom surface of the main substrate, effectively extending the coupling current path and significantly reducing the interference between antenna units. From the inside of the antenna, the orthogonally arranged Chinese character "正" shaped strips are located on the inner surface of the side dielectric substrate. From the outside of the phone, the "F" shaped patch and the Chinese character "工" shaped slot are located on the outside surface of the metal frame. Although both structures work on the same principle, the different layouts give them different functions. The "F" shaped patch and the orthogonal structure work together to form the radiating unit of the antenna.

The orthogonal arrangement of the "正" structure helps to evenly distribute the current among the feed points and improve the excitation uniformity of the antenna unit; multiple transverse and longitudinal branches provide electromagnetic energy coupling in different directions, so that the antenna unit can radiate in multiple directions and improve the coverage. At the same time with the "F" shaped patch to form a coupled feed, improve the radiation efficiency. The strong coupling between the "正" feed line branch and the "F" shaped patch forms a non-direct contact feed, which helps to optimize impedance matching and enhance the resonance mode. The "F" shaped patch is loaded on the outer surface of the side substrate, while the "正" shaped feed structure is located on the inner surface, and the two are electromagnetically coupled for energy transfer. As the structure forms multiple resonant paths, it helps the antenna achieve better impedance matching and higher gain in the 5G band. At the same time, the orthogonal arrangement of the "正" feed branches can support dual polarisation modes (e.g., horizontal and vertical polarisations), thus increasing the polarisation diversity of the MIMO antenna. In 5G terminals,

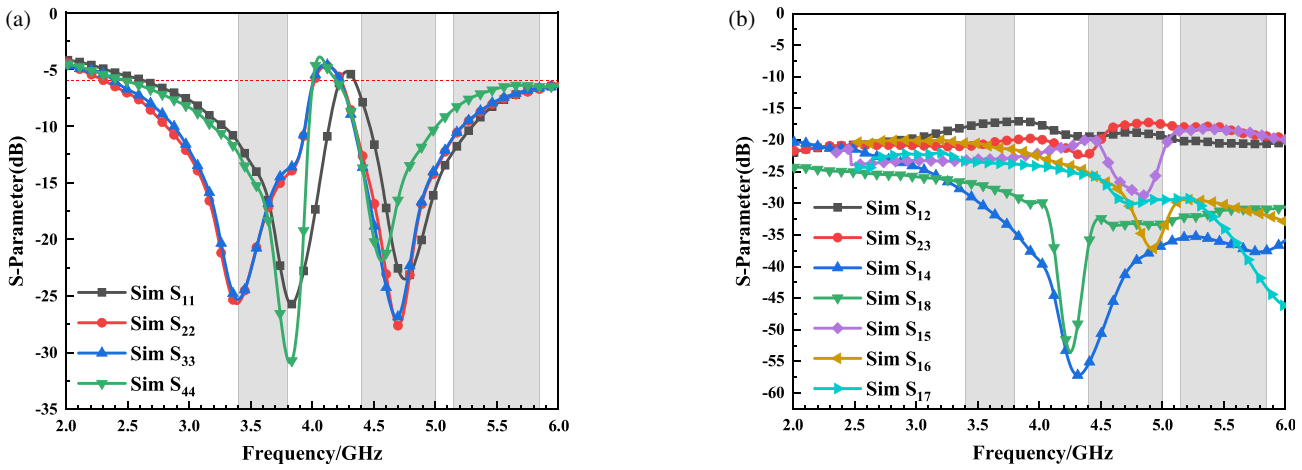

FIGURE 2. S-parameters. (a) Reflection coefficients that were simulated. (b) Transmission coefficients that were simulated.

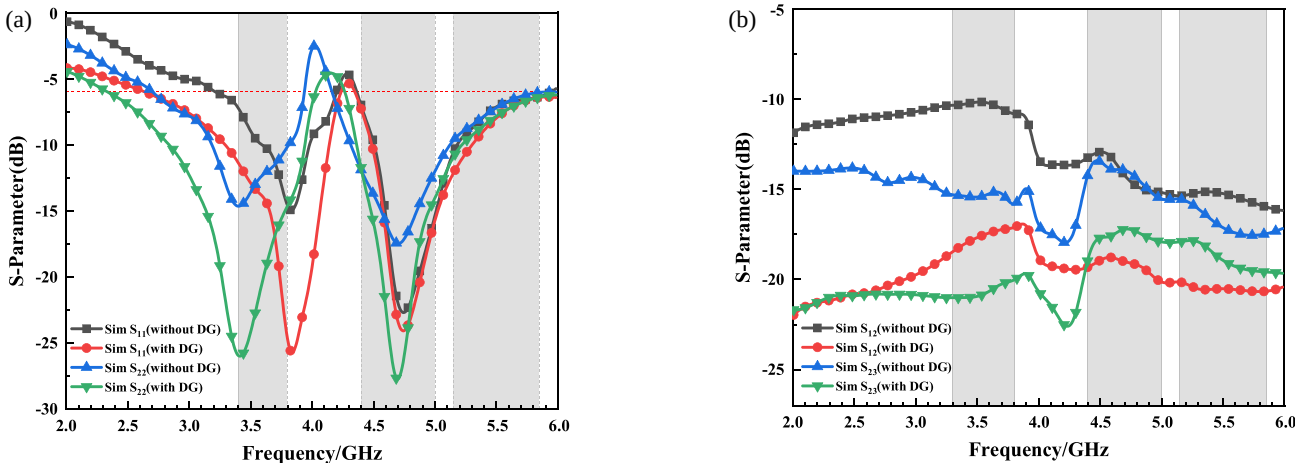

FIGURE 3. Comparison of simulated (a) Reflection coefficients, (b) Transmission coefficients between the antenna without decoupling structures and the proposed antenna.

this design reduces the correlation between antenna units and improves data transmission and interference immunity.

Due to the different locations and radiation environments of each antenna unit, the reflection coefficients will be slightly different even if they have the same dimensions. Since the antenna units have the same size and structure and are symmetrically distributed on both sides of the decoupling structure, these eight units can be divided into two groups: Ant 1, Ant 4, Ant 5, and Ant 8 belong to one group, and the remaining four antennas are categorized into the other group. Therefore, only the reflection coefficients of Ant 1, Ant 2, Ant 3, and Ant 4 are shown in Fig. 2(a). The antennas operate in the frequency bands of 2.62–3.94 GHz and 4.35–5.98 GHz, and are able to effectively cover the 5G Chinese N78 band (3.4–3.8 GHz), N79 band (4.4–5.0 GHz), and WLAN 5G band (5.15–5.85 GHz). In this paper, S_{18} denotes the transmission coefficient between Ant 1 and Ant 8, which satisfies the following relationship: $S_{18} = S_{45}$, $S_{12} = S_{34} = S_{56} = S_{78}$, $S_{23} = S_{67}$, and $S_{14} = S_{58}$. Fig. 2(b) demonstrates the isolation performance of the antenna, with all ports having more than 15 dB isolation to ensure the independence of the antenna units from each other and to avoid the interference effectively.

External decoupling structures are often used between antenna units to improve isolation and reduce correlation. In 8-element MIMO antenna designs, ground plane slits are a common means of creating equivalent circuits similar to parallel RLC configurations, which can trigger resonances at specific frequencies, adjust surface current distributions, and alter transmission characteristics. It has been shown that these slits not only enhance the isolation between cells, but also serve as functional areas for frequency spreading. Fig. 3(a) compares the reflection coefficients with and without DGS and shows that even without DGS, S_{11} and S_{22} still cover the target band, but with the addition of the defected ground structure, the impedance matching is optimized, and the bandwidth is increased. Fig. 3(b) shows the effect of the defected ground structure on the isolation performance. With the introduction of DGS, the mutual coupling is significantly suppressed; the isolation between Ant 1 and Ant 2 is significantly improved; and S_{12} and S_{23} meet the 15 dB requirement in the target band.

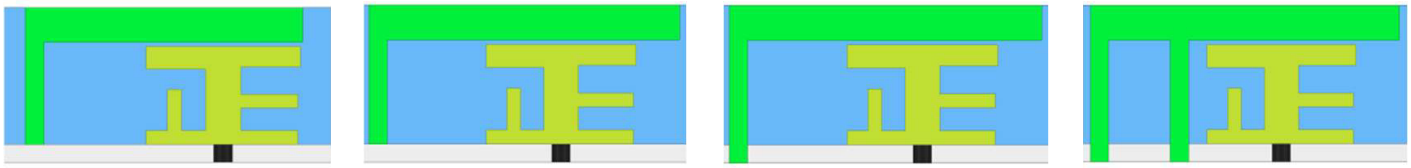

FIGURE 4. Four cases of the antenna element during the evolution process.

2.3. Design Process

The design methodology of the antenna element is shown in Fig. 4, which illustrates in detail the layout of the key structures as well as the whole process of optimization. The geometrical features of the antenna elements are visualized, and the specific functions of the components and their roles in the overall structure are also illustrated. Fig. 5 includes the simulated reflection coefficients of the antenna element to evaluate the performance of the design and its frequency response characteristics.

Figure 5 shows the variation of reflection coefficient during antenna evolution. From the simulation results, the reflection coefficient curves of Case 1 and Case 2 show that the low-frequency resonance is mainly triggered by the extension of the horizontal rectangular part of the F-shaped microstrip line loaded on the outside of the side panel. This structure optimizes the resonance characteristics in the low-frequency band by increasing the effective electrical length, thus ensuring that the antenna can maintain reliable operation in the range of 2.62–3.94 GHz. Meanwhile, the simulation results of Case 3 show that the short-circuit structure between the longitudinal rectangular portion of the F-shaped microstrip line loaded on the outside of the side panel and the ground plane plays a key role in the high-frequency resonance. The short-circuit structure effectively improves the high-frequency resonance point by adjusting the equivalent impedance of the antenna as well as the current path, covering the high-frequency band of 4.35–5.98 GHz. Ultimately, through reasonable structural design and fine optimization, the antenna element achieves comprehensive coverage of the 2.62–3.94 GHz low-frequency band and 4.35–5.98 GHz high-frequency band. This frequency response characteristic not only demonstrates the practical applicability of the antenna design, but also shows excellent band isolation performance and efficient resonance characteristics, which lays a solid foundation for the research and application of future antenna systems.

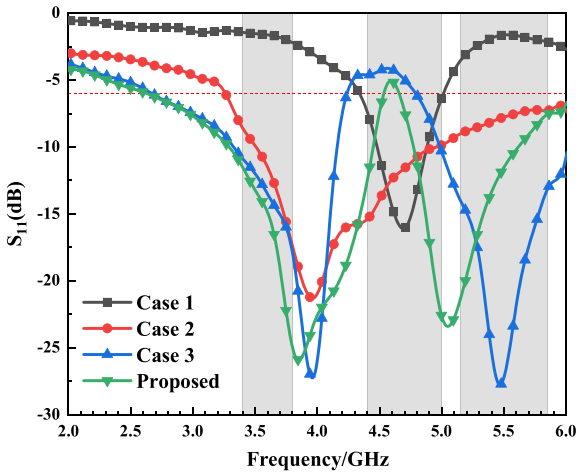

FIGURE 5. Simulated reflection coefficients of antenna elements during the evolution of antenna elements.

In order to show the working principle of the antenna more clearly, the current distribution of each antenna unit is presented in Fig. 6. Specifically, the current distribution of Ant 1 is shown in Fig. 6(a), and the strong current is mainly concentrated in the middle of the F-shaped microstrip line, near the horizontal rectangular microstrip line. The length of this strong current is about 26 mm, which is consistent with the quarter-wavelength at 3.6 GHz frequency, indicating that the antenna is in the quarter-wavelength operating mode at this resonant frequency. In addition to this, Fig. 6(b) shows the current distribution around each antenna cell when only Ant 1 is excited. From the figure, it can be observed that, except for the stronger current around Ant 1, the current intensity around the rest of the antenna units is significantly lower, which indicates that each antenna unit has a high degree of isolation and very little interference with each other, thus effectively improving the overall performance of the antenna system.

3. RESULTS AND DISCUSSION

3.1. Proposed Antenna Design

To evaluate the actual performance of the antenna, an 8-element antenna array was designed and processed, and its physical top view is shown in Fig. 7. The 8-element MIMO antenna system was fully simulated and analyzed using ANSYS software, focusing on evaluating its S-parameters, isolation, and radiation performance. Meanwhile, the S-parameters of the actual antenna are measured using a vector network analyzer to verify the accuracy of the simulation results. The far-field performance tests are conducted in an anechoic chamber to ensure low interference and high accuracy in the testing environment. In addition, key parameters such as the antenna's directional map and efficiency are also experimentally verified. The corresponding results and performance comparisons will be presented and discussed in detail later.

3.2. S-Parameters

As shown in Figs. 8(a) and (b), the antenna model is tested in a microwave darkroom to obtain its actual reflection coefficient and isolation. Since the 8-cell array antenna is symmetrically

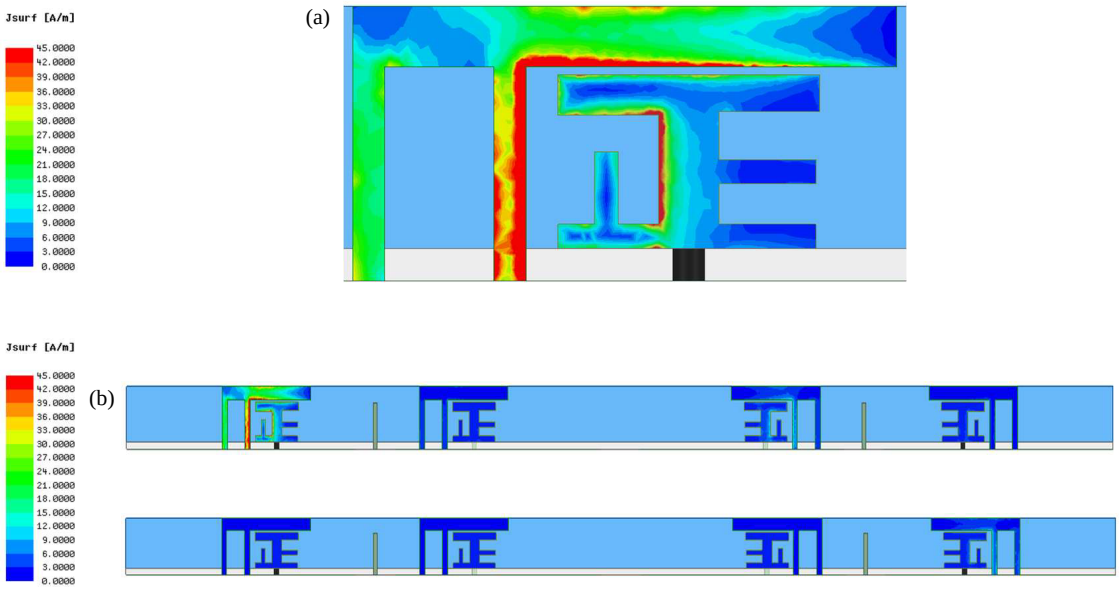

FIGURE 6. Current distribution of the antenna system when excited. (a) Current distribution of Ant 1. (b) Current distribution of each antenna unit.

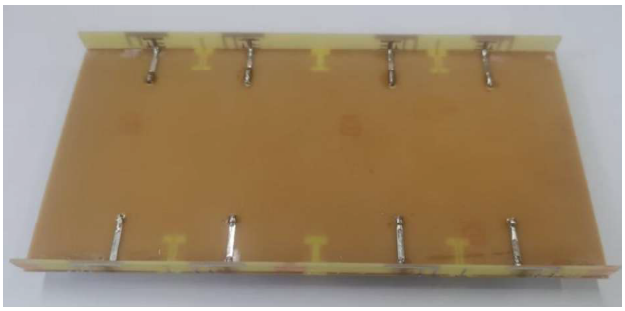

FIGURE 7. Fabricated prototype.

distributed on both sides of the metal frame, only the simulated and measured S-parameter values of one side are shown here. Fig. 9 shows the simulated and measured results of the reflection coefficient, and there are some differences between them, which are mainly manifested in the slight right shift of the resonant frequency. For example, the resonant frequency of S_{11} is 3.6 GHz in the simulation, while the measured value is 3.8 GHz, and the corresponding reflection coefficient coverage changes from 2.6–6.0 GHz to 2.8–5.8 GHz. The S_{22} also undergoes a rightward shift in resonance frequency in the low frequency section, with the resonance frequency changing from 3.4 GHz to 3.6 GHz, which suggests that the actual fabrication accuracy needs to be improved, and the deviation may be caused by the fabrication process or measurement errors. A number of solutions have been proposed to address the errors generated. Firstly, check whether the dielectric constant and thickness of the substrate material are consistent with the design value, and stricter quality control or more accurate materials can be used. Secondly, printed circuit board (PCB) or metal deposition process may lead to increased conductor surface roughness, affecting the high frequency response, and low roughness copper foil can be selected, or the plating process can be optimised. Finally, check for processing errors, such as etching accuracy and soldering inhomogeneity, and use higher precision build equipment or correct process parameters.

Meanwhile, it can be observed from the figure that the impedance bandwidths of Ant 2 and Ant 3 are slightly lower than those of Ant 1 and Ant 4, which is mainly because they are located in the middle region of the ground plane, sandwiched on both sides by the other antenna units. However, the actual measured reflection coefficients still cover the target bands, including N78, N79 and WLAN 5G, which meet the design requirements. In terms of isolation, the measured results are slightly lower than the simulated values. For example, the simulated value of S_{12} is -17 dB, while the measured value is -12.5 dB, and the difference can be attributed to the measurement accuracy. However, the measured results show that the isolation between neighboring ports is better than 10 dB, which indicates that the antenna has good port multiplexing capability and meets the MIMO antenna communication standard.

3.3. Radiation Performance

Figure 10 shows the peak gain plot of the antenna, from which we can see that the gain of the antenna designed in this paper is greater than 2 dBi throughout the operating frequency range, which shows excellent radiation performance. The simulated and actually measured radiation direction diagrams of Ant 1–Ant 4 are shown in Fig. 11, respectively, demonstrating the radiation characteristics in the xoz and yoz planes. From the xoz radiation plane, the high-gain radiation directions of Ant 1–Ant 4 are mainly concentrated at 90° and 270°, which indicates that the antenna has a strong directional radiation capability in this plane. On the other hand, in the yoz plane, the antenna is able to effectively produce omnidirectional radiation characteristics, which is suitable for application scenarios that require full coverage.

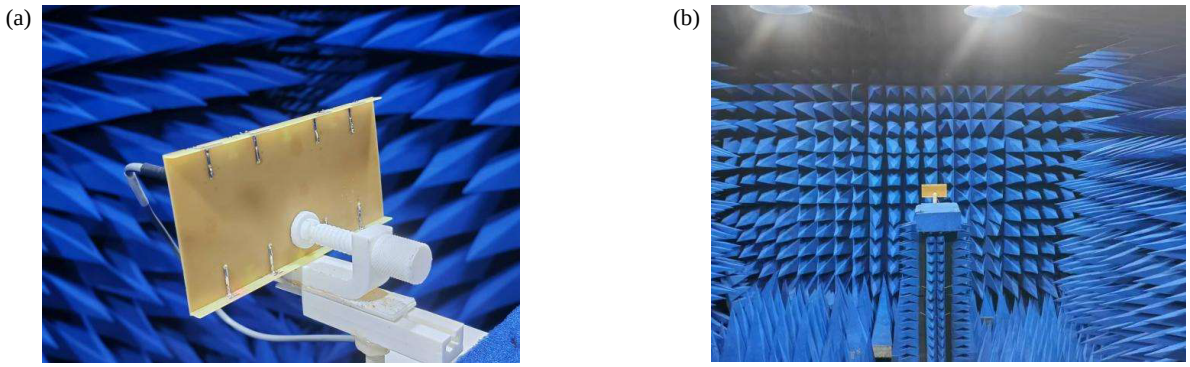

FIGURE 8. Diagram for measuring the anechoic chamber in an antenna model. (a) Overall view. (b) Far-field test environment.

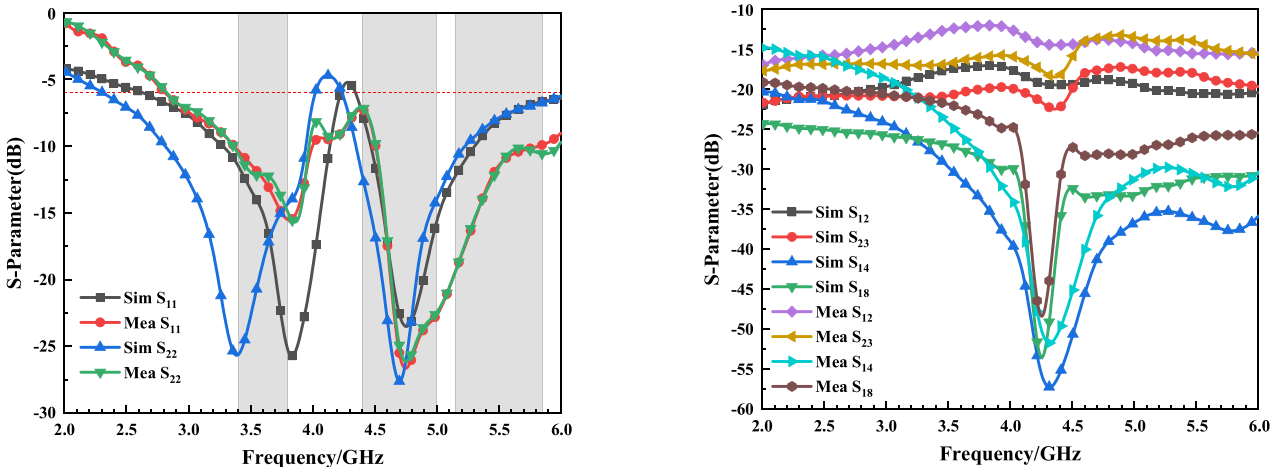

FIGURE 9. S-parameters. (a) Reflection coefficients that were simulated and measured. (b) Transmission coefficients that were simulated and measured.

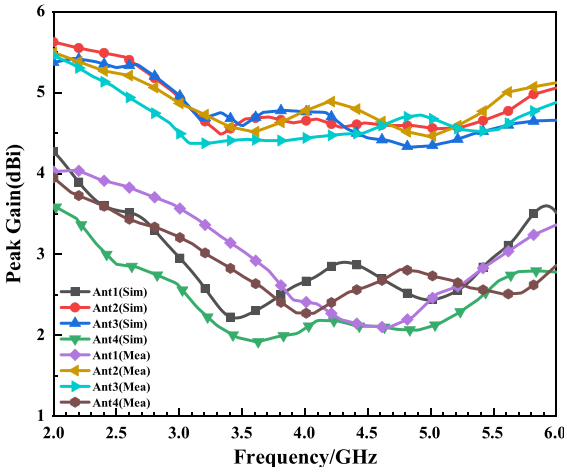

FIGURE 10. Simulated (Sim) and measured (Mea) peak gain values of Ant 1, Ant 2, Ant 3, and Ant 4.

Due to the mirror image distribution of the antenna elements, the design allows the radiation in different directions to complement each other, thus optimizing the far-field radiation characteristics and ensuring uniformity of radiation. This design helps to improve the overall performance of the antenna, especially in multi-user environments, providing more stable signal coverage. However, the differences in test environments lead to unavoidable errors between simulation and actual measurement results, which may be related to the processing of the antenna as well as the accuracy of the measurement equipment.

4. DIVERSITY PERFORMANCE

MIMO antenna's exceptional diversity qualities offer better fading and interference immunity, enabling the independent operation of each antenna. This section provides a detailed description and investigation of MIMO antenna diversity performance in terms of ECC, total active reflection coefficient (TARC), and diversity gain (DG).

4.1. Envelope Correlation Coefficient

ECC is a key parameter to measure the performance of radial directional map diversity of MIMO antennas. The correlation quality of an antenna is indicated by the ECC value. A lower ECC value usually means that the antennas are less coupled to each other, and a single antenna has less influence on other antennas, thus contributing to the overall performance of the MIMO system. MIMO antennas used in modern mobile ter-

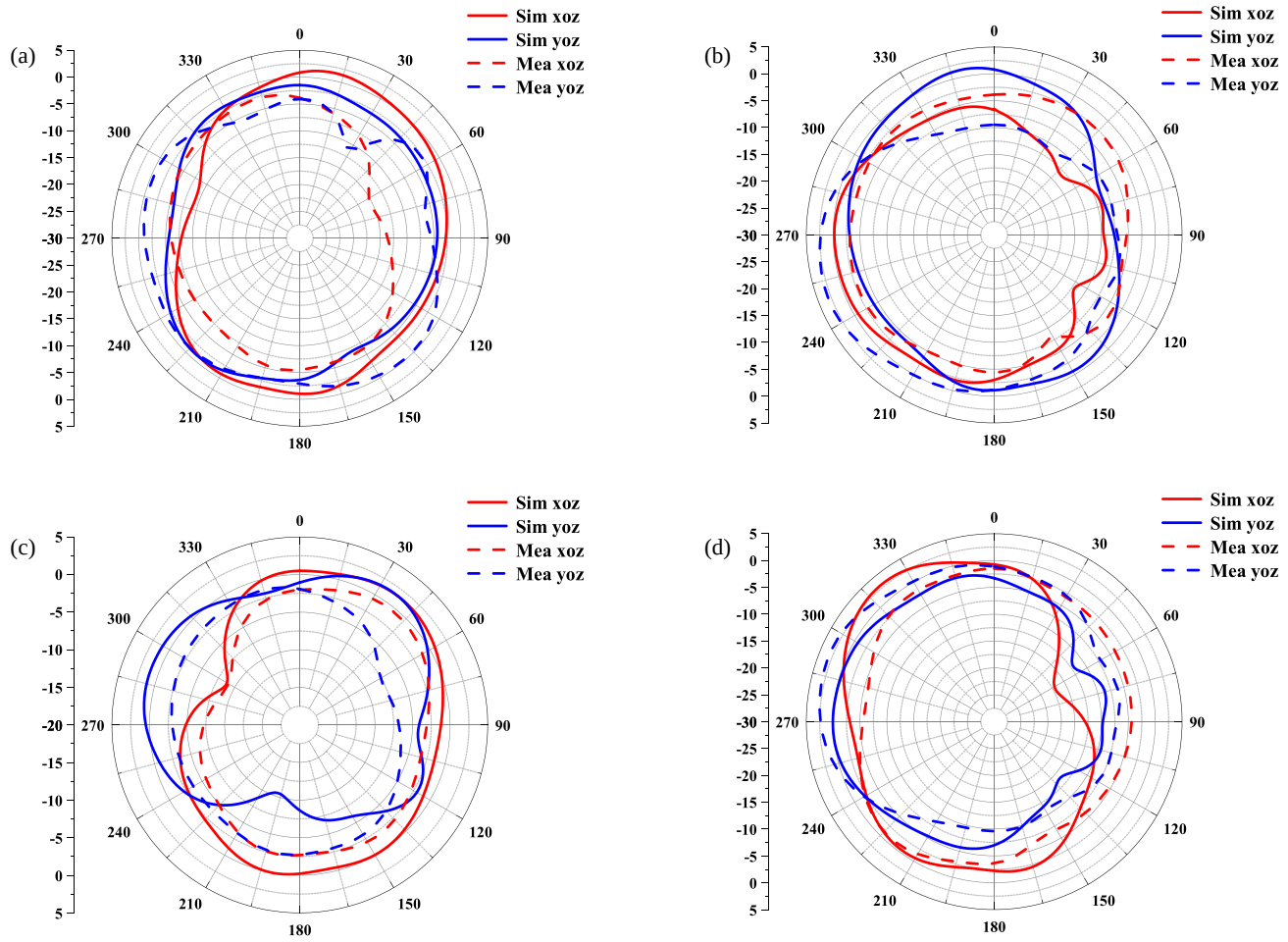

FIGURE 11. Simulated and measured far-field patterns on: (a) xoz and yoz planes of Ant 1; (b) xoz and yoz planes of Ant 2; (c) xoz and yoz planes of Ant 3; (d) xoz and yoz planes of Ant 4.

minals should usually have an ECC value less than 0.5, and the formula for calculating ECC by simulating the radiative far field is:

$$\rho_e \approx \left| \frac{\oint\oint A_{12}(\theta,\varphi)\sin\theta d\theta d\varphi}{\oint\oint A_{11}(\theta,\varphi)\sin\theta d\theta d\varphi \cdot \oint\oint A_{22}(\theta,\varphi)\sin\theta d\theta d\varphi} \right|^2 \tag{1}$$

$$A_{ij} = E_{\theta,i}(\theta,\varphi)\cdot E^*_{\theta,j}(\theta,\varphi) + E_{\varphi,i}(\theta,\varphi)\cdot E^*_{\varphi,j}(\theta,\varphi) \tag{2}$$

In Equation (1), ρ_e stands for ECC. Moreover, the ECC value of the antenna is shown in Fig. 12, where it is below 0.2 in the frequency band, which meets the standard.

4.2. Total Active Reflection Coefficient and Channel Capacity Loss

TARC is a newly proposed metric. In MIMO systems, the measurement of TARC is directly related to the total incident and reflected power. Ideally, TARC should be zero, indicating that the antenna is able to fully receive all the incident power. The measurement of TARC is crucial for evaluating the effectiveness of a MIMO system. Equation (3) can be used to calculate the TARC for a two-port configuration.

$$\text{TARC} = \sqrt{\frac{(S_{11}+S_{12})^2 + (S_{21}+S_{22})^2}{2}} \tag{3}$$

Channel Capacity Loss (CCL) is a measure of the reduction in channel capacity during information transmission. It describes how much the actual amount of information that the channel can transmit is reduced from the theoretical maximum under a given signal transmission condition due to various factors such as interference and signal fading. The larger the value of CCL is, the more serious the impairment of the channel's efficiency and performance is. This parameter is very important for designing and optimising communication systems as it is directly related to the data transmission capacity of the system. The value of CCL is usually determined by comparing it with the theoretical channel capacity to assess the actual performance of the channel. A MIMO antenna system is considered to have met the performance requirements when the CCL is lower than 0.4 bit/s/Hz, and the value of the CCL is calculated by the following equation:

$$\text{CCL} = -\log_2 \det(\alpha^R) \tag{4}$$

$$\alpha^R = \begin{bmatrix} \alpha_{11} & \alpha_{12} \\ \alpha_{21} & \alpha_{22} \end{bmatrix} \tag{5}$$

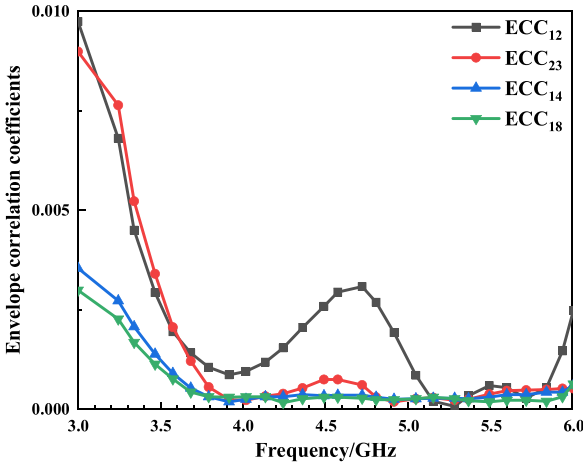

FIGURE 12. Calculated ECCs.

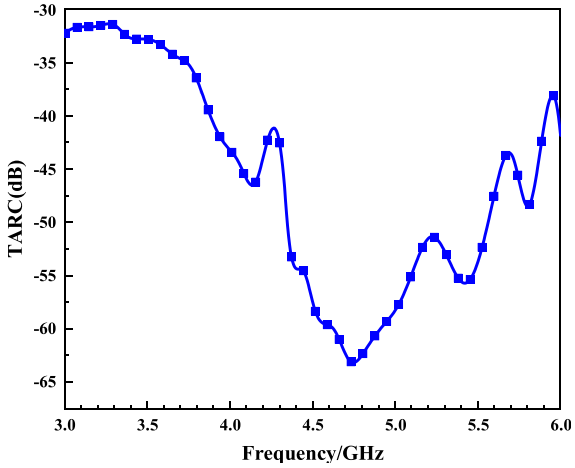

FIGURE 13. Total active reflection coefficient (TARC).

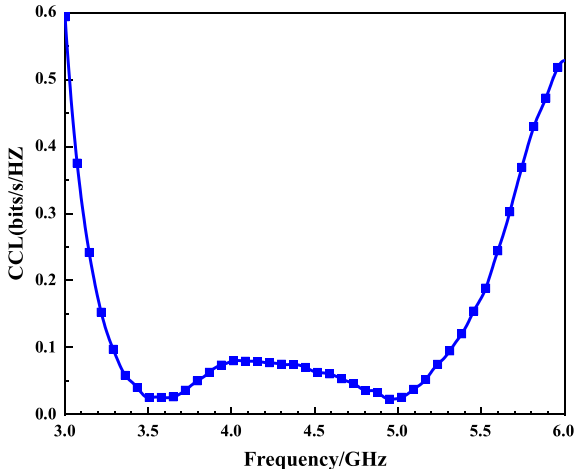

FIGURE 14. Channel capacity loss (CCL).

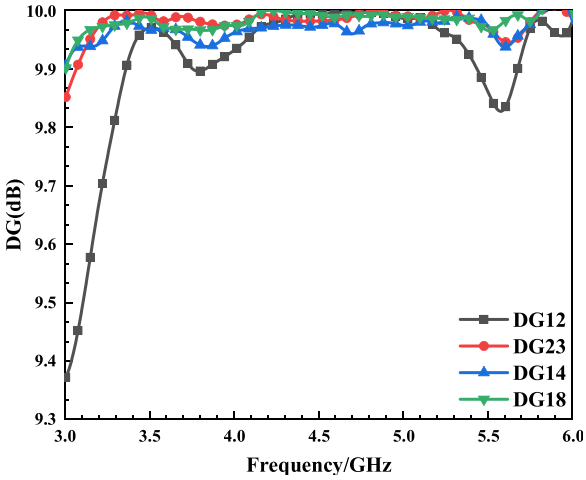

FIGURE 15. Diversity gain.

$$\begin{aligned}\alpha_{11} &= 1-(|S_{11}|^2+|S_{12}|^2);\\ \alpha_{12} &= -S_{11}*S_{12}-S_{21}*S_{22}\\ \alpha_{22} &= 1-(|S_{22}|^2+|S_{21}|^2);\\ \alpha_{21} &= -S_{22}*S_{21}-S_{12}*S_{11}\end{aligned} \tag{6}$$

Figure 13 shows the calculated TARC value of the recommended MIMO antenna, which is less than −30 dB in the operating band. Fig. 14 shows the CCL value of the MIMO antenna, which is less than 0.18 bits/s/HZ in the operating band. Therefore, the designed MIMO antenna performs well in terms of radiation efficiency and channel capacity, and can provide good signal transmission and data transmission capability.

4.3. Diversity Gain

Diversity gain (DG) is a metric used to measure diversity effectiveness. In the operating frequency range of wireless communication systems, the optimum value of DG is usually about 10 dB to ensure that the system achieves acceptable reliability. Using the ECC value, the DG can be determined by Equation (7).

Similarly, Fig. 15 illustrates the results of the DG calculation for the antenna, which shows that the MIMO antenna has a DG about 10 dB in the operating band.

$$\mathrm{DG} = 10\times\sqrt{1-|\mathrm{ECC}|} \tag{7}$$

5. PRACTICAL APPLICATION ANALYSIS

In order to investigate the performance of the antenna model in real use cases, this section discusses that the most common modes of operation for antennas embedded in smartphones are single handset mode (SHM) and dual handset mode (DHM). It is worth noting that the impact on the user's head is not discussed here since the operation is only used for data transmission and not for call mode. As shown in Fig. 16(a), only Ant 1 is kept at a certain distance from the finger, and all other antennas are in direct contact with the finger. Fig. 17 shows the radiation efficiency, transmission coefficient, and reflection coefficient of the antenna system in SHM mode. From Fig. 17(a), it can be seen that only Ant 1 has the best impedance matching of reflection coefficient, while Fig. 17(b) shows that the antenna is well

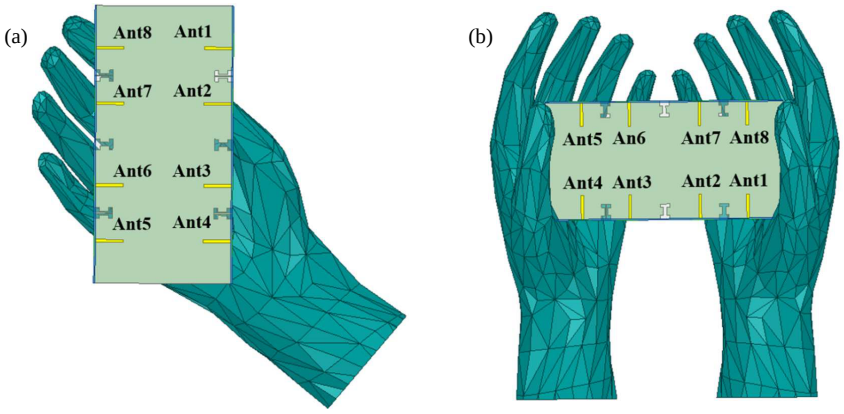

FIGURE 16. Two situations for using a portable smartphone. (a) SHM. (b) DHM.

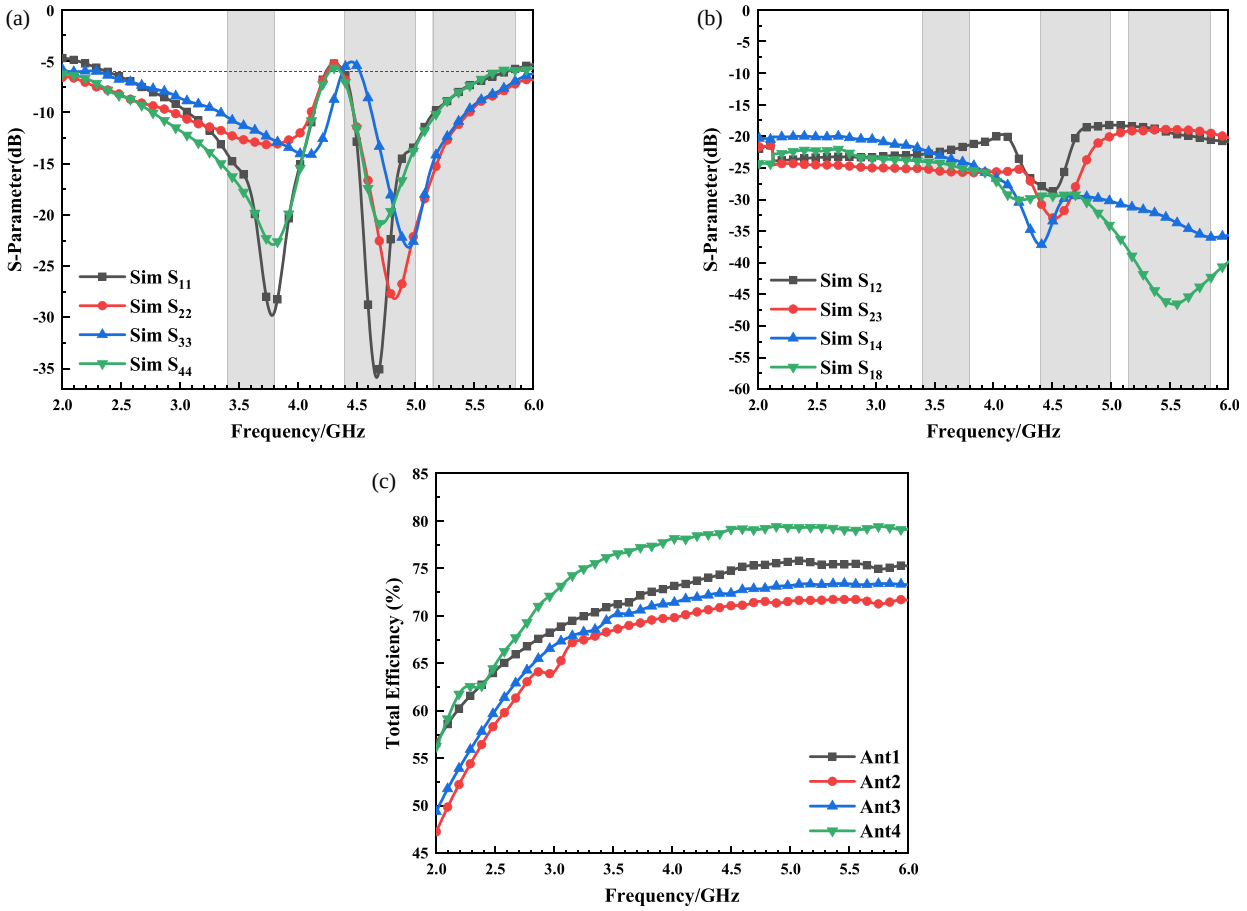

FIGURE 17. Parameters that were simulated under SHM. (a) Reflection coefficient. (b) Transmission coefficient. (c) Total efficiency.

isolated in SHM mode with transmission coefficient less than −15 dB. Fig. 17(c) shows that the efficiency of Ant 1 only decreases by about 5%, while the efficiency of the other antennas decreases by about 10%, and the efficiency of the antenna is maintained between 62% and 81% in SHM mode with good efficiency performance. Therefore, the antenna proposed in this study still has excellent performance in SHM mode.

As shown in Fig. 16(b), only Ant 2 and Ant 3 are not in direct contact with the finger, all other antennas are in direct contact with the finger. The reflection parameters under DHM are shown in Fig. 18(a), where only Ant 2 and Ant 3 are not in direct contact with the finger, while none of the other antenna elements are, and thus Ant 2 and Ant 3 clearly exhibit wider reflection coefficients. As shown in Fig. 18(b), the isolation of each port is greater than 18 dB over the entire desired operating band, which meets the isolation requirement for MIMO antenna systems. As shown in Fig. 18(c), the radiation efficiency of the antenna elements remains greater than 70% over the entire operating bandwidth, indicating that the antenna performance under DHM is also good.

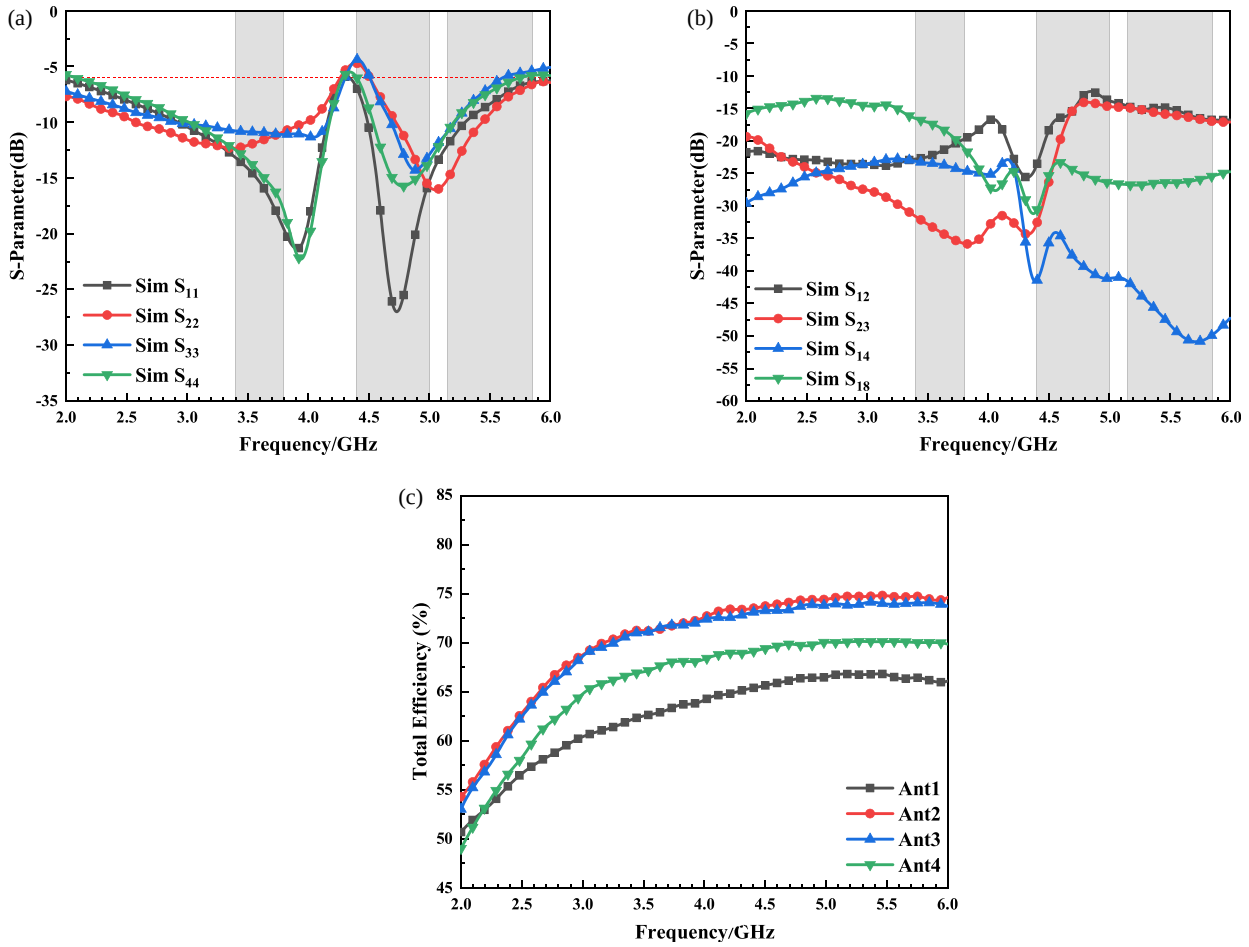

FIGURE 18. Parameters that were simulated under DHM. (a) Reflection coefficient. (b) Transmission coefficient. (c) Total efficiency.

TABLE 2. Performance comparison of 5G antenna array.

References	Bandwidth (GHz)	Isolation (dB)	ECC	Total Efficiency (%)
[2]	3.4–3.6, 4.8–6.0	15	NO	52–88
[8]	3.4–3.6	17	< 0.1	65–75
[10]	3.4–5.6	15	< 0.1	45–76
[18]	3.3–4.2, 4.8–5.0	11.5	< 0.05	52-78.5
[21]	3.25–3.90, 4.36–4.93	15	< 0.05	NO
[22]	4.45–5.52, 5.95–7.15	15	< 0.00001	> 95
This Paper	2.62–3.94, 4.35–5.98	15	< 0.01	62–79

literature [18] does not have the 5.15-5.85GHz band, literature [21] does not have the 4.4-5.0GHz, amd literature [22] does not have the 5.15-5.85 GHz"

6. COMPARISON AND DISCUSSION

The innovation of this scheme is that it proposes a new antenna structure whose antenna units are composed of the Chinese character "工", and it adopts a DGS decoupling design, which effectively reduces the coupling between antenna units and thus improves the overall performance. Table 2 shows the comparison of the designed 8-element bezel antenna with other existing schemes in terms of bandwidth, isolation, ECC, and total efficiency. Ref. [2] does not have the 3.3–3.4 GHz band; [8] does not have the 3.3–3.4 GHz, 4.8–5.0 GHz, and 5.15–5.85 GHz bands; [10] does not have the 3.3–3.4 GHz and 5.15–5.85 GHz bands; [18] does not have the 5.15–5.85 GHz band; [21] does not have the 4.4–5.0 GHz band; [22] does not have the 5.15–5.85 GHz band. Compared with the antennas in the literature [2, 8, 10, 18–20], the proposed antenna supports 5G N78/N79 and WLAN 5 GHz bands and can cover more frequency bands. Moreover, the proposed antenna achieves

−15 dB in isolation, which outperforms [15] and also outperforms the related studies in [11, 14, 15], in terms of total efficiency. This MIMO system shows strong advantages in terms of diversity and gain. In summary, the proposed design has better performance and is very suitable for application in mobile terminals in wireless communication networks. Table 2 compares the performance of the proposed MIMO antenna with other schemes in the literature.

7. CONCLUSIONS

In this paper, we propose a new 8-cell MIMO cell phone bezel antenna design tailored for 5G new radio (NR) band and WLAN 5G (5.15–5.85 GHz) band. Compared to existing solutions, the design not only offers the advantages of a simple structure and ease of fabrication, but also has significant bandwidth coverage capabilities to effectively support multiple frequency bands. The antenna units have low coupling coefficients, high antenna efficiency, and excellent diversity performance. In terms of specific design, eight functionally consistent antenna units (Ant 1–Ant 8) are integrated into the metal bezel of the smartphone to build a complete 8×8 MIMO antenna array. Each unit adopts a patch antenna structure, equipped with a $50\,\Omega$ microstrip feedline and a Chinese character "正" antenna design. In order to achieve excellent impedance matching in the high-frequency band, a tuned truncation line is added to the feedline, and a slot structure is designed on the substrate. The design successfully achieves full coverage of the target frequency bands (2.62–3.94 GHz and 4.35–5.98 GHz), and meets the requirements of 5G N78/N79 bands and WLAN 5 GHz bands at the same time. Experimental results show that the design delivers excellent performance, including mutual coupling rejection of more than −15 dB, good far-field radiation patterns, envelope correlation coefficients below 0.01, and high efficiencies of 62%–79%, providing a reliable solution for 5G mobile terminals.

ACKNOWLEDGEMENT

This work was supported in part the Natural Science Research Project of Anhui Educational Committee under grant No. 2022AH051583, No. 2022AH052138 and No. 2023AH052650, in part by the Anhui Province Graduate Academic Innovation Project under grant No. 2023xscx074, in part by the Funding Project of Scientific Research Starting for the High-level Talents of West Anhui University under grant No. WGKQ2022009.

REFERENCES

[1] Fu, Z. and W. Shen, "Eight-element self-decoupled MIMO antenna design for 5G smartphones," *International Journal of RF and Microwave Computer-Aided Engineering*, Vol. 31, No. 3, e22523, Jan. 2021.

[2] Wang, Y., X. Wang, J. Wang, and R. Shao, "Dual-band highly isolated eight-element MIMO antenna for 5G mobile phone," *Applied Computational Electromagnetics Society Journal (ACES)*, Vol. 37, No. 5, 588–596, 2022.

[3] Sun, L., H. Feng, Y. Li, and Z. Zhang, "Compact 5G MIMO mobile phone antennas with tightly arranged orthogonal-mode pairs," *IEEE Transactions on Antennas and Propagation*, Vol. 66, No. 11, 6364–6369, 2018.

[4] Deng, C., D. Liu, and X. Lv, "Tightly arranged four-element MIMO antennas for 5G mobile terminals," *IEEE Transactions on Antennas and Propagation*, Vol. 67, No. 10, 6353–6361, 2019.

[5] Dong, J., S. Wang, and J. Mo, "Design of a twelve-port MIMO antenna system for multi-mode 4G/5G smartphone applications based on characteristic mode analysis," *IEEE Access*, Vol. 8, 90 751–90 759, 2020.

[6] Zhao, A. and Z. Ren, "Multiple-input and multiple-output antenna system with self-isolated antenna element for fifth-generation mobile terminals," *Microwave and Optical Technology Letters*, Vol. 61, No. 1, 20–27, 2019.

[7] Gurjar, R., D. K. Upadhyay, B. K. Kanaujia, and A. Kumar, "A compact modified Sierpinski carpet fractal UWB MIMO antenna with square-shaped funnel-like ground stub," *AEU — International Journal of Electronics and Communications*, Vol. 117, 153126, 2020.

[8] Guo, Y., J. Xue, and L. Zhao, "Decoupling of MIMO antenna with dummy antennas for 5G mobile terminals," in *2022 International Applied Computational Electromagnetics Society Symposium (ACES-China)*, 1–2, Xuzhou, China, 2022.

[9] Du, K., Y. Wang, L. Zhang, and Y. Hu, "Design of wideband decoupling antenna pairs for 5G portable devices at N77/N78/N79 bands," *Micromachines*, Vol. 13, No. 11, 1964, 2022.

[10] Hei, Y. Q., J. G. He, and W. T. Li, "Wideband decoupled 8-element MIMO antenna for 5G mobile terminal applications," *IEEE Antennas and Wireless Propagation Letters*, Vol. 20, No. 8, 1448–1452, 2021.

[11] Chou, J.-H., J.-F. Chang, D.-B. Lin, and T.-L. Wu, "Dual-band WLAN MIMO antenna with a decoupling element for full-metallic bottom cover tablet computer applications," *Microwave and Optical Technology Letters*, Vol. 60, No. 5, 1245–1251, 2018.

[12] Li, Y., C.-Y.-D. Sim, Y. Luo, and G. Yang, "High-isolation 3.5 GHz eight-antenna MIMO array using balanced open-slot antenna element for 5G smartphones," *IEEE Transactions on Antennas and Propagation*, Vol. 67, No. 6, 3820–3830, 2019.

[13] Wong, K.-L., J.-Y. Lu, L.-Y. Chen, W.-Y. Li, and Y.-L. Ban, "8-antenna and 16-antenna arrays using the quad-antenna linear array as a building block for the 3.5-GHz LTE MIMO operation in the smartphone," *Microwave and Optical Technology Letters*, Vol. 58, No. 1, 174–181, 2016.

[14] Chang, L., Y. Yu, K. Wei, and H. Wang, "Polarization-orthogonal co-frequency dual antenna pair suitable for 5G MIMO smartphone with metallic bezels," *IEEE Transactions on Antennas and Propagation*, Vol. 67, No. 8, 5212–5220, 2019.

[15] Sun, L., Y. Li, Z. Zhang, and H. Wang, "Self-decoupled MIMO antenna pair with shared radiator for 5G smartphones," *IEEE Transactions on Antennas and Propagation*, Vol. 68, No. 5, 3423–3432, 2020.

[16] Chou, J.-H., J.-F. Chang, D.-B. Lin, and T.-L. Wu, "Dual-band WLAN MIMO antenna with a decoupling element for full-metallic bottom cover tablet computer applications," *Microwave and Optical Technology Letters*, Vol. 60, No. 5, 1245–1251, 2018.

[17] Li, Y., C.-Y.-D. Sim, Y. Luo, and G. Yang, "High-isolation 3.5 GHz eight-antenna MIMO array using balanced open-slot antenna element for 5G smartphones," *IEEE Transactions on Antennas and Propagation*, Vol. 67, No. 6, 3820–3830, 2019.

[18] Cui, L., J. Guo, Y. Liu, and C.-Y.-D. Sim, "An 8-element dual-band MIMO antenna with decoupling stub for 5G smartphone

applications," *IEEE Antennas and Wireless Propagation Letters*, Vol. 18, No. 10, 2095–2099, 2019.

[19] Wang, Z., M. Li, M. Yang, W. Nie, W. Mu, H. Lin, and Z. Lu, "Design of wideband 8-element MIMO mobile phone antenna based on sub-6 GHz NR band," *Progress In Electromagnetics Research C*, Vol. 129, 187–201, 2023.

[20] Cheng, B. and Z. Du, "Dual polarization MIMO antenna for 5G mobile phone applications," *IEEE Transactions on Antennas and Propagation*, Vol. 69, No. 7, 4160–4165, 2021.

[21] Addepalli, T., M. Sharma, M. S. Kumar, N. K. Gollamudi, P. R. Kapula, and C. M. Kumar, "Self-isolated miniaturized four-port multiband 5G sub 6 GHz MIMO antenna exclusively for N77/N78 & N79 wireless band applications," *Wireless Networks*, Vol. 30, No. 2, 1037–1053, 2024.

[22] Addepalli, T., V. S. Nagaraju, S. Medasani, J. C. Rao, P. Badugu, C. M. Kumar, R. Uppada, and B. K. Kumar, "Four-element equilateral triangular-shaped MIMO antenna with connected ground for 5G sub: 6 GHz N79 and WiFi-6E band applications," *International Journal of Communication Systems*, Vol. 37, No. 16, e5895, 2024.